JOURNAL OF MATERIALS SCIENCE 28 (1993) 4775–4780

Laser cladding of high-temperature coatings

J. DE DAMBORENEA, A.J. VÁZQUEZ
Centro Nacional de Investigaciones Metalúrgicas (CENIM), Avenida de Gregorio del Amo 8, E-28040 Madrid, Spain

The processing and microstructural characteristics of nickel-based superalloys obtained by high-power laser surface cladding were studied. The processing variables were laser power, scan velocity and the composition of the feeder powder. The initial compositions consisted of a mixture of NiCrAl (71/18/11 % by weight) and NiCrAl plus zirconium oxide composite (66/16/12/4 % by weight). Following the process, the clad layers were characterized using analytical tools such as optical and scanning electron microscopy and thickness, substrate/coating interface, cracks and their hardness.

1. Introduction

Over the last two decades, there have been spectacular changes in the design and use of new high-temperature resistant materials. The clearest examples are gas turbine engines in which the new operating conditions, based on an increase in temperature and working pressure, require new materials that are capable of withstanding such extreme conditions. Advances in the development of these materials have been partly responsible for the fact that, if the working temperature in 1940 was 700 °C, in the 1960s it was over 950 °C, and currently is 1350 °C. New models of higher turbine entry temperatures (TETs) operate at 1550 °C, while working temperatures of around 1700 °C are expected to be achieved shortly [1, 2].

This situation is accompanied by joint tension and temperature problems, making the choice of material a critical aspect. The search for new materials has mainly been focused on the use and modification of several types of superalloys (nickel-, chromium- or iron-based), and the inclusion of ceramic materials which act as thermal barriers to prevent the degradation of the alloy.

This search has been accompanied by the improvement of superalloy production processes: from arc- and air-induction melting in the early years, to vacuum-induction melting and refining in the late 1950s, and the current use of consumable-electrode remelting [3]. The recent introduction of high-density energy techniques, such as the electron beam and the laser, which permit very fast solidification, open new possibilities in the production of such alloys. In 1975, Glenny *et al.* [4] claimed that the future of this type of material would be directly linked to the cooling capacity of the superalloy production processes.

In a previous paper [5], the results of processing NiCrAl alloys on carbon steel were presented. In this new phase, changes have been made to both the variables controlling the process (beam power, feed rate and speed) and the initial composition of powder feed and base material. After the process, the clad layers were examined in order to determine their thickness, the existence of cracks and/or delaminations, substrate/coating interface and hardness.

2. Experimental procedure

Surface cladding was carried out using a Spectra-Physics transversal flow CO_2 laser with a 10.6 μm wavelength, operating in multimode form, with a variable power of between 3000 and 5000 W.

The output beam diameter from the optical cavity was 44 mm, focusing with a 7.5 in (~ 19 cm) lens to a diameter of 8 mm, and supplying a spot area of 64 mm^2. The process was carried out under a gaseous argon process, with a flow of 30 l min^{-1}. The experimental conditions were fixed after several initial tests using powers of 3, 4 and 5 kW. The use of 5000 W on the piece was most favourable.

Surface cladding on NiCrAl-based alloys was produced using the particle-injection technique described elsewhere in the literature [6].

The powders used were mixtures of nickel, chromium and aluminium with and without the addition of zirconium oxide composite. The powders were the same as the type normally used in plasma deposition processes, with an average particle size of between 45 and 75 μm. After weighing, they were kiln dried at 120 °C for 50 h, and then mixed by mechanical shaking to ensure perfect homogenization of the mixture.

The initial composition of the test mixtures is shown in Table I. The zirconium composite corresponded to a Metco 202NS, with a composition of 80 % by weight of zirconium oxide and 20 % yttrium oxide, from which the corresponding part was taken to achieve the desired composition. The zirconium is added to increase the solid-solution hardening and is a suitable replacement for other expensive rare-earths such as hafnium.

TABLE I Composition of the alloys

Alloy	Element (wt %)				
	Ni	Cr	Al	Zr	Y
I	71	18	11	–	–
II	66	16	12	3	1

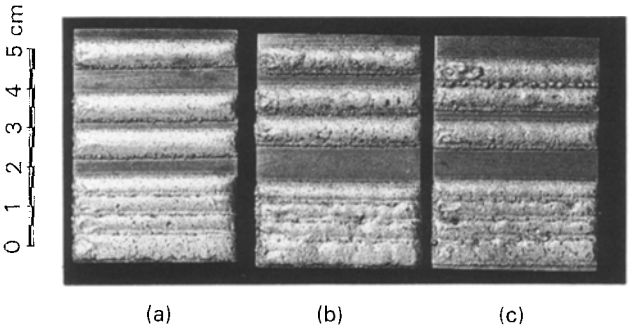

Figure 1 General appearance of NiCrAl-clad layers processed at (a) 65 g min^{-1} and 700 mm min^{-1}, (b) 75 g min^{-1} and 700 mm min^{-1}, and (c) 75 g min^{-1} and 1000 mm min^{-1}.

Powder feeding was by means of a Metco injector with incorporated balance, permitting constant monitoring of the feed flow. Flows of 65, 75 and 95 g min^{-1} were used.

The beam sweep over the piece was controlled using a computer-controlled two-axis table. Speeds were 500, 700 and 1000 mm min^{-1}.

The particle-injection technique permitted the production of both simple and overlapped tracks. In the latter case, an overlap of 50 % was used.

In all cases, the base material was 316L stainless steel with a composition of 16 % Ni, 12.5 % Cr, 2.5 % Mo and a carbon content of less than 0.05 %.

Optical microscopy and scanning electron microscopy with EDS X-ray analysis were used for the microstructural analyses.

3. Results and discussion

The general appearance of the clad layers is good, with no problems of adherence or external cracks on the coating. This aspect is shown (Fig. 1) for the Alloy I specimens processed at a power of 5000 W and different flows and speeds. The coating is generally homogeneous and regular, as seen in Fig. 2 for one overlapped sample with the above conditions.

The coating thickness is, for simple belts, a function of both feed flow and sweep speed. Its linear variation with flow rate is shown in Fig. 3, for a fixed speed of 700 mm min^{-1}. As may be expected, the higher the flow, the greater the thickness. The tracks obtained at a powder feed of 95 g min^{-1} are extremely irregular, even when their production speed is changed, making them unsuitable for use. The micrographic detail of these belts (Fig. 4) shows the results at 700 (upper), 1000 (centre) and 500 mm min^{-1} (lower). In the latter case, the belt has a better aspect, probably due to the longer beam–powder interaction time, which facilitates greater powder melting. Nevertheless, its form remains irregular.

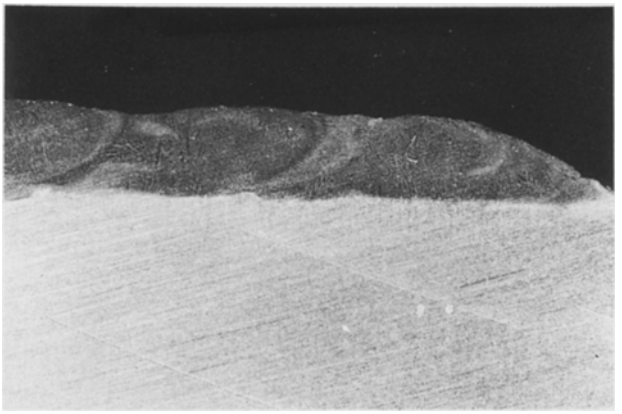

Figure 2 Transverse macrograph (×7) of an overlapped sample processed at 5000 W, 65 g min^{-1} and 700 mm min^{-1}.

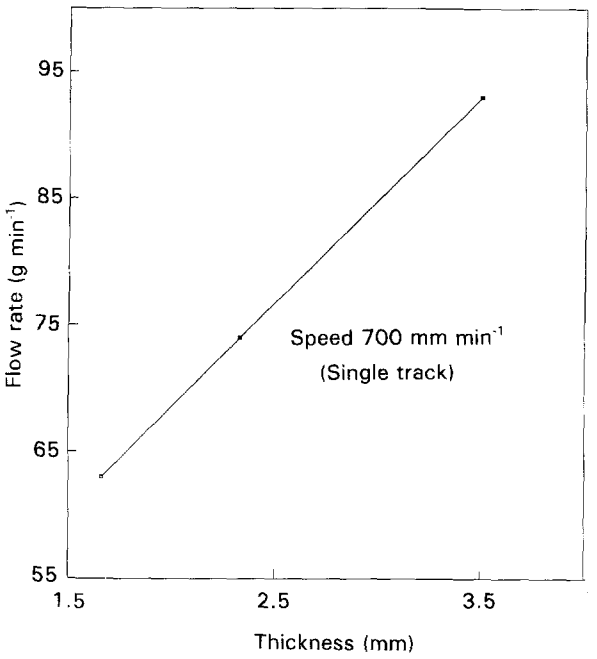

Figure 3 Variation of thickness as a function of flow rate for a single track.

The result for a set flow of 75 g min^{-1} is shown in Fig. 5 as a variation of layer thickness with speed. Predictably again, the higher the sweep speed, the lower the thickness. Of all the test conditions, the best results were obtained at speeds of 500 and 700 mm min^{-1} and flows of 75 g min^{-1}.

In the case of specimens processed at 500 mm min^{-1}, the composition of the resultant layer is practically the same as that of the initial powders, with a composition in the external part of 68.5 % Ni, 18 % Cr, 7.5 % Al and 6 % Fe (wt %). The average distribution of the elements constituting the cladding was uniform throughout the laser-clad region. The variation in the track composition from the base steel to the external surface is presented in Fig. 6.

The metallographic structures resulting from the surface cladding process are similar in all cases, as

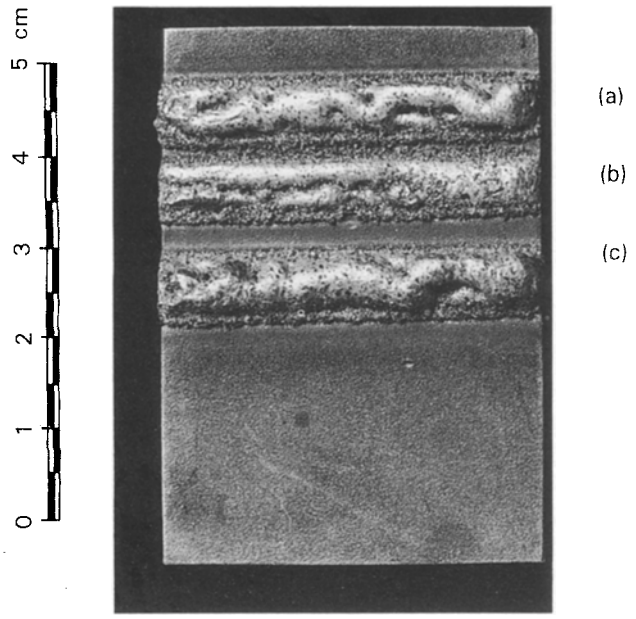

Figure 4 External aspect of laser cladding at 95 g min^{-1} and (a) 700 mm min^{-1}, (b) 1000 mm min^{-1}, and (c) 500 mm min^{-1}.

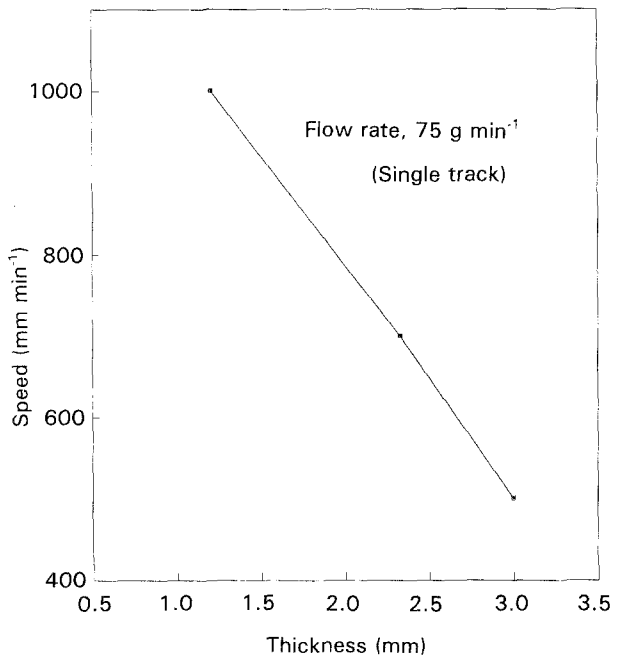

Figure 5 Thickness variation as a function of beam speed.

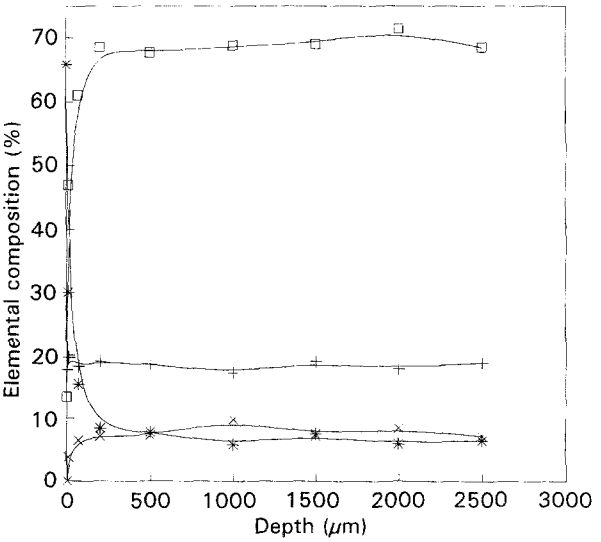

Figure 6 X-ray microanalysis of the coating from the substrate/coating interface to the top of the track. (+) Cr, (*) Fe, (□) Ni, (×) Al.

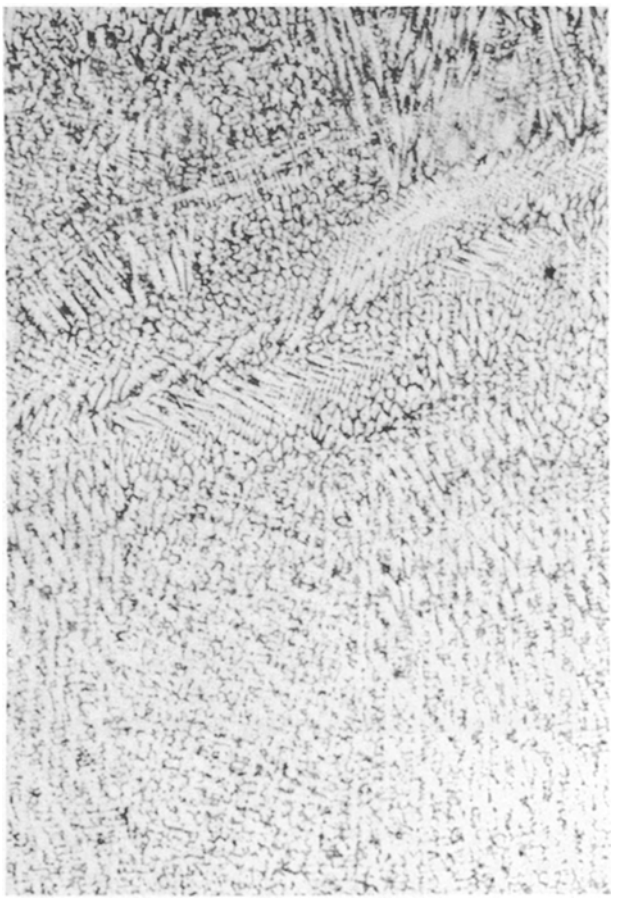

Figure 7 Typical metallographic structure of the surface-clad layers (× 50).

shown in a representative case in Fig. 7. The coating/stainless steel base interface (Fig. 8) is a continuum without imperfections or heterogeneities. This reveals the existence of a good metallurgical bond between the base and the supply material. Immediately after this interface, there is a zone in which a smudged dendritic structure can be made out with a second phase approximately 30 μm below on the edges. This second phase is shown in Fig. 9. The material thus consists of a matrix and a second phase.

Following analysis in the electronic microprobe, the matrix is seen to be a solid solution of nickel with chromium, iron and aluminium, equivalent to phase γ. The second phase has a composition of 25 % atomic weight aluminium, 55 % atomic weight nickel, while the rest is iron and chromium. This seems to indicate the formation of phase γ′, i.e. the Ni_3Al intermetallic. Under normal conditions of solidification, the nickel-based superalloys exhibit phase γ′ after suitably long ageing heat treatments. In this case, however, an activation for the precipitation of this phase seems to exist. This activation must be in the effect of other

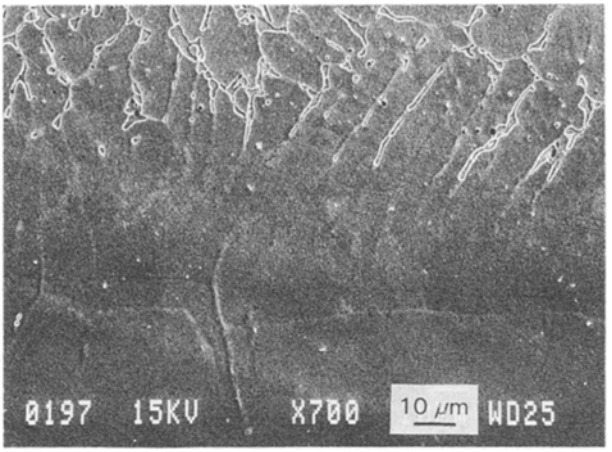

Figure 8 Detail of the substrate/coating interface.

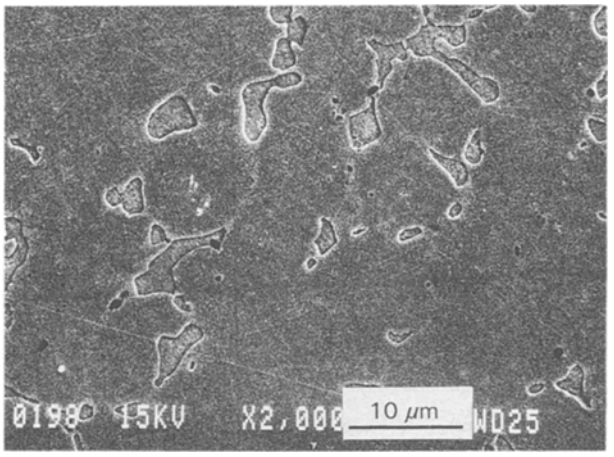

Figure 9 Detailed structure of the NiCrAl alloy.

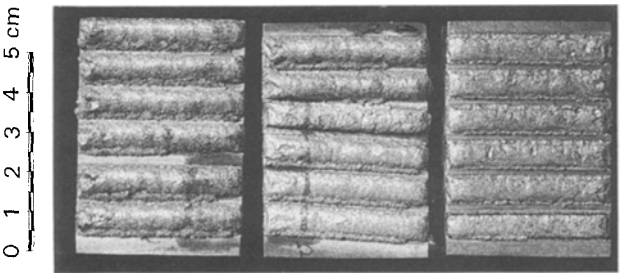

Figure 10 External appearance of NiCrAl + zirconium composite-clad layers processed at (a) 75 g min^{-1} and 500 mm min^{-1}, (b) 75 g min^{-1} and 700 mm min^{-1} and (c) 75 g min^{-1} and 1000 mm min^{-1}.

alloying elements. From the results of the heat treatment during the process, a dilution from the substrate occurs of certain amounts of other alloy elements, as iron, present at the clad layer. According to Singh and Mazumder [7] iron can substitute both nickel and aluminium in the γ' (Ni_3Al) phase. Therefore, it seems that at certain concentrations, iron acts in NiCrAl types of alloy in the same way as rare-earths, such as hafnium, i.e. its addition enhances the activation energy or driving force for the precipitation of Ni_3Al. Under these conditions, a possible composition of the γ' precipitate would be $(NiCrFe)_3Al$. These results are similar to those found in a previous study [5], which showed that a dilution of up to almost 25 at % of iron occurred during the melting process. In the present case, the dilution is considerably lower (around 8 at %), but enough to affect the formation of that phase.

The aspect of the specimens in Alloy II is shown in Fig. 10. Their metallographic structure is similar to the others, with a matrix, γ, and a dispersed Ni_3Al phase, although there is a notable precipitation of the ceramic composite on the edges of the latter phase (Fig. 11). This is because during cladding, the mixture of oxides combines to form a stabilized zirconium that provides better thermal stability and greater heat-shock resistance. A qualitative analysis of each phase using the electron microprobe revealed the contents in each element as shown in Table II. As can be seen, the white-point composition (near 44 at %) corresponds to Zr_2O_3, the balance is oxygen.

As in the previous case, the metal/coating interface is presented as a continuum (Fig. 12). The white spots, which are distributed uniformly throughout the specimen, are zirconium rich. The presence of Y_2O_3 was not detected, however. Under these conditions, it ought to react also with the aluminium to form a ductile ceramic oxide that should improve the cohesion of the coating at a high temperature. We believe that its non-detection was due to the limitations of the analysis technique.

Specimens of both Alloys I and II exhibit occasional intergranular cracks, with a growth from the surface

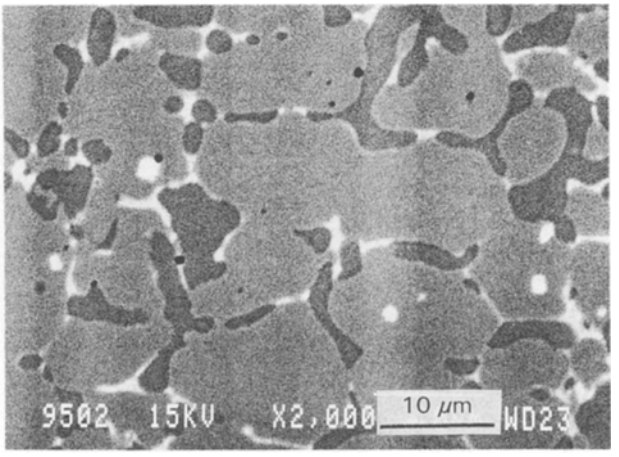

Figure 11 General survey of the matrix, intermetallic compound and zirconium oxide.

TABLE II Qualitative analysis of the phases

	Element (wt %)					
	Ni	Cr	Al	Zr	Fe	Y
Matrix	67	18	6	–	9.9	–
Second phase	70	11	14	–	5.5	–
White points	7.4	2.8	1.8	73.9	1.2	–

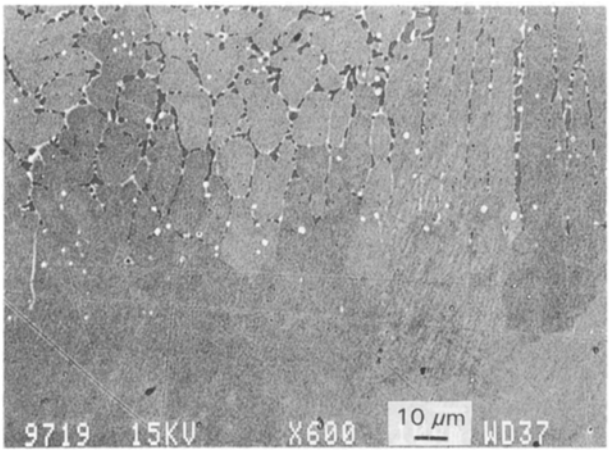

Figure 12 Substrate/coating interface for NiCrAl + zirconium composite.

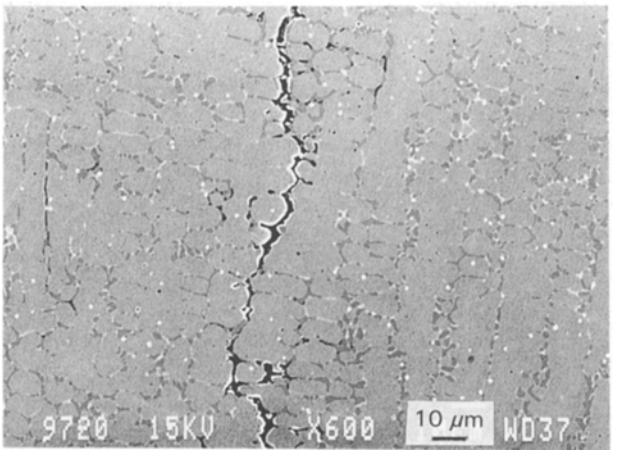

Figure 13 Light micrograph of laser-clad layer showing cracking.

inwards and also from immediately above the metal/coating interface towards the track. These cracks seem to be due to the high solidification speed, which causes high tension in the coating. This phenomenon is more accentuated in the specimens processed at the highest speed (1000 mm min^{-1}) and in those of Alloy II. In the latter case (Fig. 13), the cracks follow the trajectory of the zirconium particles beside the phase γ'. Their appearance has the same explanation as in Alloy I, although the existence of ceramic oxides generates a higher temperature gradient, which favours the appearance of thermal stress. In spite of the cracks, delamination from the substrate was not observed in any case.

These cracks are found in much smaller proportions in the specimens processed at lower speeds and in the overlapped specimens. In the latter case, the explanation must be sought in a thermal effect derived from the high energy density of the laser beam. This forces a thermal treatment over the substrate at the same time as the process, resulting in a preheating of the specimen.

According to the literature [8], preheating temperatures for ZrO_2 should be around 1050 °C. In the present case, however, it should be recalled that the ceramic material used in the alloy is only 4 % of the total in weight, permitting lower preheating. Good adherence and cracking resistance have been achieved in other types of ceramic coatings such as SiO_2, even at only 400 °C [9]. Vandehaar *et al.* [10], working with zirconium and alumina cladding on UDIMET 700 superalloys and AISI 4140 steel, also suggest that preheating the substrate reduces the stress accompanying the process and eliminates spallation.

The hardness of both types of alloy was measured. Under equal processing conditions, Alloy II is harder than Alloy I. Its variation along a cross-section of the belt is shown in Fig. 14. Although the material cannot be considered to be hard, there is a degree of increase that is probably due to the presence of the ceramic oxides. The resultant values of hardness are, nevertheless, consistent with those suggested in the literature [10] for these types of layers.

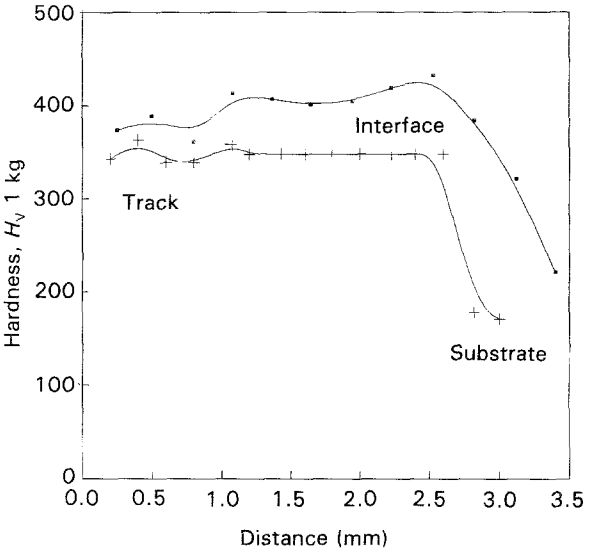

Figure 14 Hardness of the different laser-cladding alloys. (□) NiCrAl + YPSZ, (+) NiCrAl.

In conclusion, the surface laser cladding of nickel alloys on to stainless steel were examined, fixing the optimum parameters for the processing. The clad layers were characterized by means of optical and scanning microscopy showing a matrix of solid-solution of nickel (γ) plus intermetallic Ni_3Al. No delamination of the coating was observed, although some cracking appeared overall, following the γ' phase, when the ceramic oxide was present. The corrosion behaviour of these alloys under electrochemical and high-temperature oxidation is currently being examined.

Acknowledgement

The authors thank the Interministerial Commission for Science and Technology (CICYT) for funding the project MAT88-0144 which was responsible for financing this study.

References

1. J. STRINGER, *Mater. Sci. Technol.* **3** (1987) 482.
2. T. KHAN, *Adv. Mater. Process* **1** (1990) 19.
3. C. H. WHITE, P. M. W ILLIAMS and M. MORLEY, *ibid.* **4** (1990) 53.
4. R. J. E. GLENNY, J. E. NORTHWOOD and A. BURWOOD-SMITH, *Int. Metall. Rev.* **20** (1975) 1.
5. J. J. de DAMBORENEA and A. J. VÁZQUEZ, *J. Mater. Sci.* **27** (1992) 1271.
6. V. M. WEERASINGHE and W. M. STEEN, in "Applied Laser Tooling", edited by M. Soares and M. Perez-Amor (Martinus Nijhoff, Dordrecht, 1987) p. 183.
7. J. SINGH and J. MAZUMDER, *Metall. Trans.* **19A** (1988) 1981.
8. B. L. MORDIKE, in "Processing of Metals and Alloys", edited by R. W. Cahn (VCH, Berlin, 1991) p. 112.
9. J. de DAMBORENEA and F. ZUBIRI, to be presented at 10th European Corrosion Congress, Barcelona, 5–8 July 1993.
10. E. VANDERHAAR, P. A. MOLIAN and M. BALDWIN, *Surface Eng.* **4** (1988) 159.

Received 19 August 1992
and accepted 25 February 1993